第 35 卷第 10 期 无 机 化 学 学 报 Vol.35 No.10
2019 年 10 月 CHINESE JOURNAL OF INORGANIC CHEMISTRY 1834-1842

金属有机框架衍生的高性能锂离子电池负极 Co_3O_4/C 复合材料

苟 蕾* 赵少攀 刘鹏刚 杨江帆 樊小勇 李东林*
(长安大学材料科学与工程学院,新能源材料与器件研究所,西安 710061)

摘要:为克服 Co_3O_4 负极材料导电率低、循环稳定性差的缺点,选择 $Co_2(NDC)_2DMF_2$(NDC=1,4-萘二甲酸根)为前驱体采用两步煅烧工艺,制备了具有高碳含量的 Co_3O_4/C 复合材料。采用 X 射线衍射(XRD)、扫描电子显微镜(SEM)、X 射线光电子能谱(XPS)和拉曼光谱对样品进行了表征。采用热重分析法(TGA)测定了 Co_3O_4/C 中非晶态碳的含量。作为锂离子电池的负极材料,Co_3O_4/C 具有高的可逆比容量、优异的循环性能(在 200 mA·g^{-1} 的电流密度下,循环 200 圈后放电比容量稳定保持在 1 000 mAh·g^{-1})和良好的倍率性能(在 100、200、500、1 000 和 2 000 mA·g^{-1} 的电流密度下,放电比容量为分别 1 076.3、976.2、872.9、783.6 和 670.1 mAh·g^{-1})。材料优异的电化学性能归结为有机配体衍生的高含量非晶态碳的导电和缓冲作用有利于电子的快速传递并有效减缓了金属氧化物充放电过程中的体积膨胀。

关键词:电化学;锂离子电池;负极;复合材料;Co_3O_4;MOF
中图分类号:O611.3 **文献标识码**:A **文章编号**:1001-4861(2019)10-1834-09
DOI:10.11862/CJIC.2019.182

Metal-Organic Framework Derived Co_3O_4/C Composite as High-Performance Anode Material for Lithium-Ion Batteries

GOU Lei* ZHAO Shao-Pan LIU Peng-Gang YANG Jiang-Fan FAN Xiao-Yong LI Dong-Lin*
(*Institute of New Energy Materials and Device, School of Materials Science and Engineering, Chang'an University, Xi'an* 710061, *China*)

Abstract: In order to overcome the disadvantages of the low electrical conductivity and poor cycling stability of Co_3O_4 anode material, a Co_3O_4/C composite was obtained by the judicious selection of $Co_2(NDC)_2DMF_2$ (NDC=1,4-naphthalene dicarboxylate) as precursor through a two-step calcination process. The sample was characterized by X-ray diffraction (XRD), scanning electronic microscopy (SEM), X-ray photoelectron spectroscopy (XPS) and Raman spectroscopy. The content of amorphous carbon in Co_3O_4/C was tested by thermogravimetric analysis (TGA). As anode material for lithium-ion batteries (LIBs), Co_3O_4/C material showed a high reversible specific capacity, remarkable cycling performance (the specific discharge capacity was stable at 1 000 mAh·g^{-1} under the current density of 200 mA·g^{-1} even after 200 cycles) and an excellent rate performance with high average discharge specific capacities of 1 076.3, 976.2, 872.9, 783.6 and 670.1 mAh·g^{-1} at 100, 200, 500, 1 000 and 2 000 mA·g^{-1}, respectively. The excellent electrochemical performance was attributed to the amorphous carbon derived from the organic ligand, which served as conductive path for easy electric charge transfer and buffer layer to slow down the volumetric stresses.

Keywords: electrochemistry; lithium-ion battery; anode; composite; Co_3O_4; MOF

收稿日期:2019-04-23。收修改稿日期:2019-06-06。
国家自然科学基金(No.21103013,21473014)、陕西省自然科学基金(No.2016JM5082)和大学生创新创业资助项目(No.201810710113,201910710469)资助。
*通信联系人。E-mail:leigou@chd.edu.cn,dlli@chd.edu.cn

0 Introduction

The global energy crisis and climate change issues have led to a vigorous exploration of electrochemical energy storage systems[1-2]. Lithium-ion batteries (LIBs) have attracted widespread attention due to their unique advantages (*e.g.*, large specific capacity, good chemical stability, high energy density, and no-memory effect)[3-5]. However, currently commercial lithium-ion batteries are approaching the limits of the theoretical capacity prediction of the electrode materials. Therefore, in order to meet the ever-increasing demands of energy, power, safety and stability requirements, it is necessary to develop a new anode material with excellent electrochemical performance[6-9]. Co_3O_4 has a theoretical capacity of 890 $mAh \cdot g^{-1}$, which is more than twice that of industrial graphite and is considered to be a promising anode material[10-15]. However, there are still some obstacles to its commercialization, including large volume changes during lithium ions insertion/extraction, which lead to serious electrode pulverization, therefore resulted in a rapid capacity decay, and poor ion and electron conductivity[16]. One effective strategy to solve the above mentioned problems is compositing transition metal oxides with conductive carbon materials, such as graphene[17-18], carbon nanotubes[19-20] and other carbon materials[21-22]. Since carbon can not only improve the conductivity of the electrode material but also function as a buffer to prevent structural collapse caused by large volume changes[23].

In recent years, metal oxides from metal-organic frameworks (MOFs) precursors have received extensive attention[24]. It is well known that MOFs as a kind of hybrid functional materials have potential applications in molecule separation, chemical sensing, heterogeneous catalysis, drug delivery and gas storage due to their diverse structures, large surface areas and adjustable pore sizes[25-29]. In addition, versatile MOFs structures can be fabricated by changing the metal nodes and organic ligands with coordination hybrid atoms providing a large number of opportunities to obtain various metals, metal oxides, metal sulfurs, metal phosphorous, carbon materials and composites[30-33]. With respect to Co_3O_4 anode materials synthesized through metal-organic frameworks as precursors′ route, ZIF-67 is one of the commonly used MOFs precursors[34-37]. Shao et al. obtained two hollow structured Co_3O_4 (ball-in-dodecahedron and concaved-odecahedron) via one-step and two-step calcination of ZIF-67, respectively[38-39]. Qu et al. prepared graphene-supported ultrafine Co_3O_4 through thermal decomposition of GO/ZIF-67[39]. In addition to ZIF-67, some other MOFs such as Prussian blue analogue $Zn_3[Co(CN)_6]_2$[40], $[Co_3(HCOO)_6]DMF$ (DMF=*N*,*N*-dimethylformamide)[41], Co-BTC (BTC=1,3,5-benzenetricarboxylate)[42], Co(1,4-BDC)(DMF) (BDC=1,4-benzenedicarboxylate)[43] have also been reported. Due to the different MOFs precursors and different calcination process were used, Co_3O_4 anodes showed different morphologies and different electrochemical performances.

We have synthesized a Co_3O_4 anode material by calcination of $Co_2(NDC)_2(DMF)_2$ (NDC=1,4-naphthalene dicarboxylate, DMF=*N*,*N*-dimethylformamide) in air, which shows a capacity of 1 058.9 $mAh \cdot g^{-1}$ after 100 cycles at a current density of 200 $mA \cdot g^{-1}$ [44]. Considering the ligand that contains a larger conjunctive system than terephthalic acid, which may contribute more carbon content during the carbonization process. Thus, in this work, we synthesized a Co_3O_4/C composite by a two-step calcination of $Co_2(NDC)_2(DMF)_2$. Compared with our previously work, this work has significantly improved the battery performance. The resulted Co_3O_4/C composite exhibited an excellent rate performance with high average discharge specific capacities, which was also superior to most reported cobalt oxides anode materials.

1 Experimental

1.1 Preparation of materials

$Co_2(NDC)_2(DMF)_2$ was synthesized according to literature[44]. Typically, 1,4-naphthalene dicarboxylic acid (1,4-H_2NDC) (1 mmol, 0.216 g) and $Co(NO_3)_2 \cdot 6H_2O$ (0.5 mmol, 0.145 g) were dissolved in *N*,*N*-dimethylformamide (DMF) (30 mL). The mixture was transferred to and sealed in a 50 mL Teflon-lined

stainless steel autoclave after 30 min stirring, kept at 130 ℃ for 48 h, and finally cooled to room temperature. The purple precipitate $Co_2(NDC)_2(DMF)_2$ was collected by centrifugation and dried at 60 ℃ in an oven for 12 h after rinsing with DMF for three times.

Co_3O_4/C composite was synthesized by a two-step calcination process that was calcining the $Co_2(NDC)_2(DMF)_2$ precursor in a tube furnace at a temperature of 800 ℃ for 3 h with a heating rate of 2 ℃·min^{-1} in argon atmosphere, then at 350 ℃ for an hour in an ambient atmosphere. As for comparison, pure Co_3O_4 was obtained by calcining Co_3O_4/C composite under 450 ℃ in air for several hours to remove the carbon component.

1.2 Characterization

The X-ray powder diffraction (XRD) mode of the product was recorded using a Bruker D8 Advance diffractometer with Cu $K\alpha$ (λ=0.154 nm) at 40 kV and 40 mA in a scanning range of 5°~70° (2θ). The content of carbon in Co_3O_4/C composite was determined by thermogravimetric analysis (TGA) was carried out using a TA SDT Q600 thermoanalyser under air flow at 10 ℃·min^{-1} from room temperature to 800 ℃. The component was confirmed by X-ray photoelectron spectroscopy (XPS) using an X-ray photoelectron spectrometer (ThermoFisher). Field-emission scanning electron microscope (FE-SEM) images were taken on Zeiss sigma 500 FE-SEM using a 5 kV focus voltage to research the morphologies of the materials. Raman spectrum was obtained using a Laser Raman spectroscopy (in Via, RENISHAW) using a 514 nm argon ion laser.

1.3 Electrochemical measurements

The electrochemical measurements of all samples were measured by fabricating CR2025 type coin cells in an argon-filled glove box. To prepare a working electrode, the as-synthesized active materials, acetylene black (Super-P) and polyvinylidene fluoride (PVDF) were mixed in *N*-mzethyl pyrrolidone (NMP) with a weight ratio of 55:35:10 to form a homogeneous slurry. The resulting slurry was pasted onto the surface of a copper foil current collector and dried at 100 ℃ in vacuum oven for 12 h. The coin cells were assembled in an argon filled glove box with the as-prepared materials as the test electrode, metallic lithium as the counter and reference electrode, 1 mol·L^{-1} $LiPF_6$ in a 1:1 (*V*/*V*) mixture of ethylene carbonate (EC) and dimethyl carbonate (DMC) as the electrolyte, and Celgard 2400 micro-porous membrane as the separator. After standing for 24 h, the galvanostatic charge-discharge and rate tests were carried out on a new Neware current test system with a voltage range of 0.01 to 3 V. The cyclic voltammetry (CV) measurements were performed at the Versa STAT3 electrochemical workstation with a measurement range of 0.01 to 3 V and a scan rate of 0.1 mV·s^{-1}. Electrochemical impedance spectroscopy (EIS) measurements were performed using a Versa STAT3 electrochemical workstation with a frequency range of 100 kHz to 10 mHz and a signal amplitude of 5 mV.

2 Results and discussion

2.1 Synthesis of Co_3O_4/C composite

$Co_2(NDC)_2(DMF)_2$ was used as the precursor to obtain Co_3O_4/C composite due to a higher carbon content could be obtained after calcination where the naphthalene had a larger conjugated ring than benzene ring. The experimental process was shown as Fig.1.

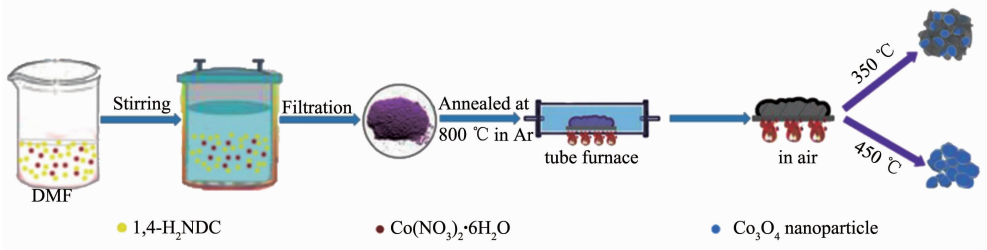

Fig.1 Diagram of the synthesis of Co_3O_4/C

2.2 Characterization

The X-ray diffraction (XRD) pattern of $Co_2(NDC)_2(DMF)_2$ was in good agreement with the literature[44], indicating successful synthesis of the precursor (Fig.

S1). After two-step calcination, the purple precursor was converted to a black sample, which was also characterized by XRD analysis. As shown in Fig.2a, all diffraction peaks of 19°, 31.27°, 36.85°, 38.54°, 44.81°, 55.65°, 59.36°, 65.65°, 68.6°, and 69.73° could be used as the unique index of Co_3O_4 (PDF No. 42-1467). There was no diffraction peak of carbon detected in the XRD pattern, indicating that the decomposed carbon may exist in the form of amorphous state. The existence of amorphous carbon was further confirmed by Raman spectrum due to the strong D band peak (Fig.2b).

The final residual carbon content was determined by TGA measurement at a heating rate of 10 ℃·min^{-1} in air, as shown in Fig.2c. There were two distinct stages of weightlessness. The occurrence of a weight loss of about 0.5% below 200 ℃ could be attributed to the release of the absorbed gases or moisture on the surface of the Co_3O_4/C composite. Then an abrupt weight loss indicated that amorphous carbon has burned out before the temperature increased to 650 ℃. When the temperature was raised above 650 ℃, the residue content remained constant. Thus, the carbon content in Co_3O_4/carbon composite was calculated to be 14.47%(*w*/*w*).

The surface composition of Co_3O_4/C was characterized by XPS (Fig.3). The typical characteristic peaks on the full map are clearly visible (Fig.3a), the characteristic peaks of 284.43, 530.35, 780.24 eV corresponded to the characteristic peaks of C1*s*, O1*s* and Co2*p*, respectively, confirming that C, O, and Co were the main elements in the samples. The existence of C element which was attributed to the residues from the decomposition of organic ligands. The convolutional Co2*p* spectrum is depicted in Fig.3b. There were two strong peaks at 779.76 and 794.93 eV, respectively, corresponding to the Co2$p_{3/2}$ and Co2$p_{1/2}$ spin-orbital peaks of Co_3O_4, respectively[45-47]. The energy separation between Co2$p_{3/2}$ and Co2$p_{1/2}$ was approximately 15 eV, which was consistent with the standard Co_3O_4 spectra[46-49]. It can be seen from the spectrum of C1*s* that the main carbon peak at 284.43 eV belonged to amorphous carbon in Fig.3c. The peak at 284.7 eV was designated to C-C/C =C contamination, which often led to a significant asymmetry in the graphitized C1*s* peak towards higher binding energy, which confirmed the presence of carbon to some extent. The peak positions were 286.4 and 290.1 eV, respectively, due to the presence of C-O and O-C=O[46-47,50-51], indicating the presence of carbon and oxygen-containing functional groups. Fig.3d showed the de-volume XPS spectrum of the O1*s* with three different peaks at 533.1 (C-OH), 531.2 (O-C), and 530 eV (O=C-OH)[46-47].

Fig.4 showed the SEM images of Co_3O_4/C composite. As can be seen from Fig.4a, the sample maintained the same block-shaped structure as the precursor (Fig.S2). As shown in Fig.4b, it can be clearly seen that these micro-sized blocks were not as dense as the precursor, and the surface of the block was not as smooth as the precursor, which formed some cracks. It can be seen from the high magnification SEM images (Fig.4c) that the micro-scale blocks were composed of a large number of nanoparticles and tiny void spaces between particles, which is beneficial to the diffusion of the electrolyte. The corresponding

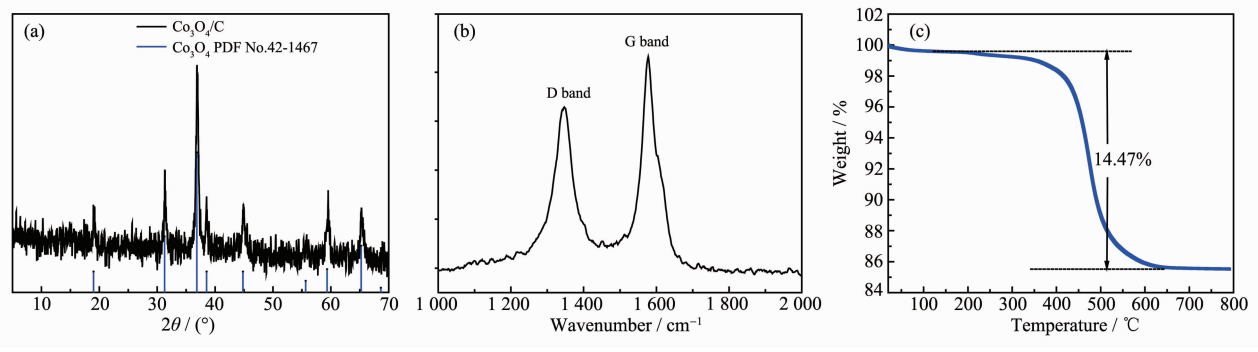

Fig.2　XRD pattern (a), Raman spectrum (b) and TGA curve (c) for the Co_3O_4/C composite

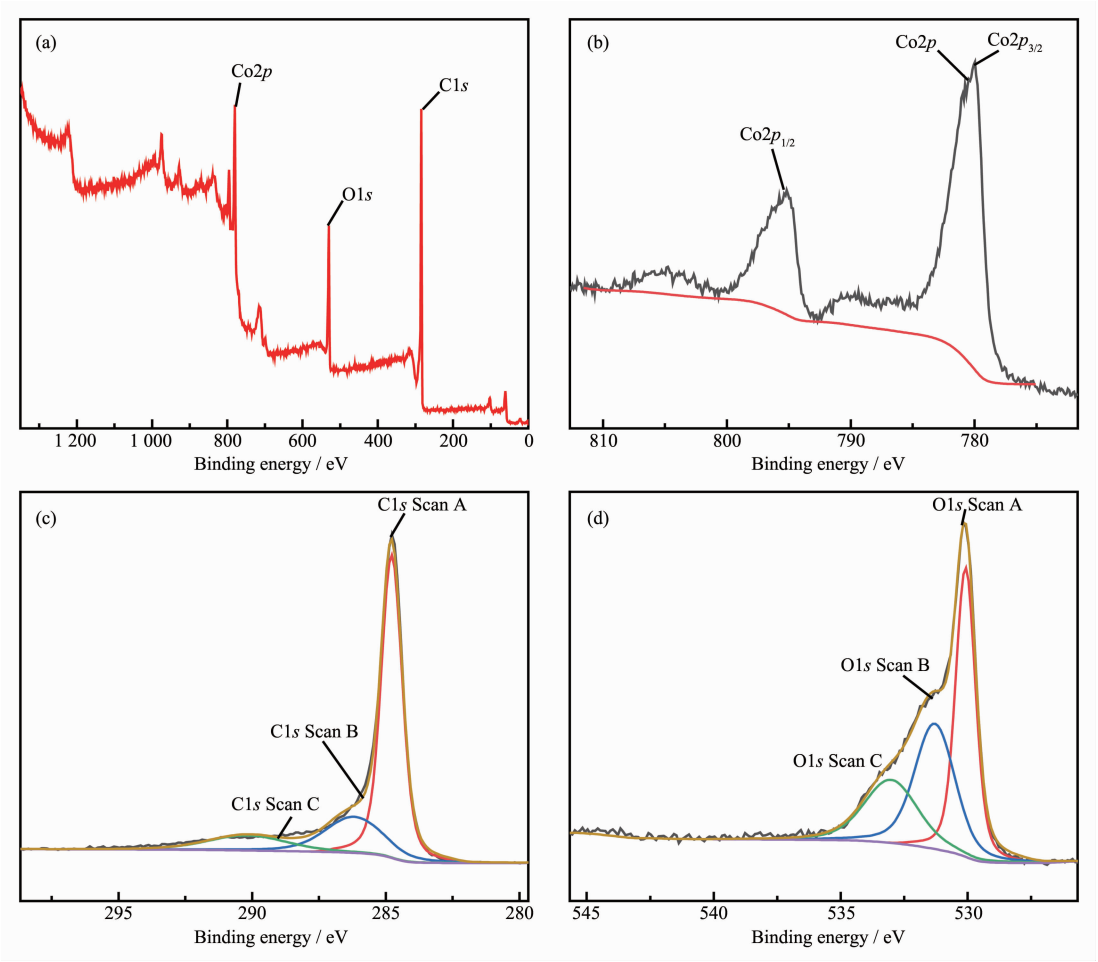

Fig.3 XPS survey spectra of the Co_3O_4/C (a), XPS spectra of Co2*p* (b), XPS spectra of C1*s* (c) and XPS spectra of O1*s* (d)

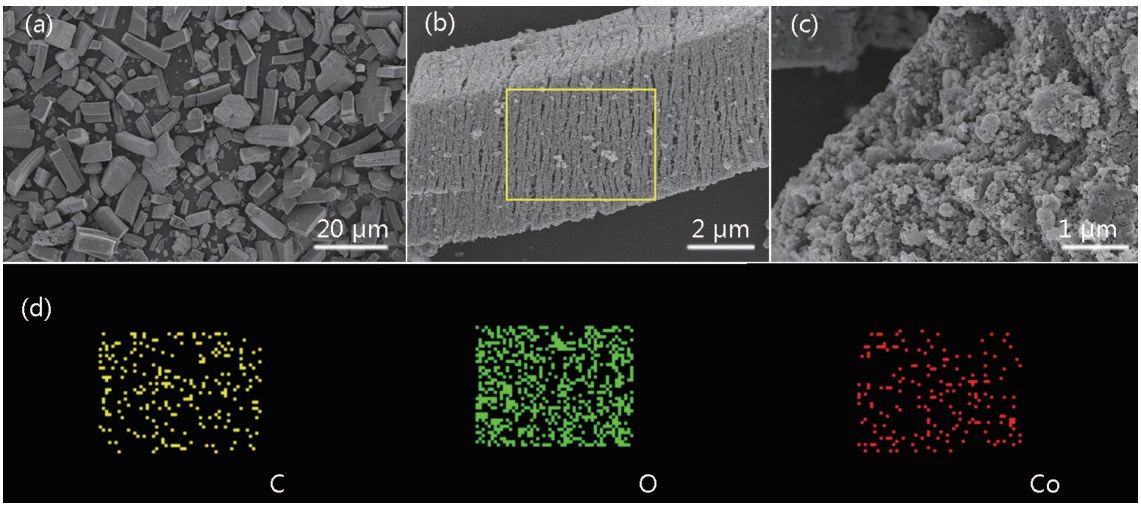

Fig.4 SEM images of Co_3O_4/C composite at different magnifications (a~c) and corresponding elemental mapping (d)

elemental mapping shown in Fig.4d indicated the existence of Co, O and C. We deduced that Co_3O_4 particles were uniformly dispersed into the carbon network.

2.3 Electrochemical properties

Fig.5 showed the cyclic voltammogram (CV) of the first three cycles of Co_3O_4/C at a voltage range of 0.01 to 3 V and a scan rate of 0.1 mV·s^{-1}. In the first

cycle, two strong cathodic peaks appeared at 0.6~0.75 V due to the initial reduction of cobalt metal by Co_3O_4 during discharge. A multi-step electrochemical reduction reaction of Co_3O_4 with metal Co ($Co_3O_4+8Li^++8e^- \rightarrow 4Li_2O+3Co$)[52-53] formed a partially irreversible solid electrolyte interface (SEI)[53-54]. A broad oxidation peak of about 2.1 V occurred during the charging process due to the oxidation of cobalt into Co_3O_4 and Li_2O decomposition. From the second cycle, the reduction peak moved to about 1.1 V, and the position of the oxidation peak did not deviate too much. This was still the formation of clusters and the formation of Co_3O_4 phase between the metal Co and Li_2O in the conversion reaction[52,55-56]. In the subsequent cycles, the intensity and voltage position of main cathode and anode peaks showed a good overlap, indicating that the insertion and extraction reactions had good reversibility. The result showed that the electrochemical reversibility of Co_3O_4/C gradually formed after the initial cycle.

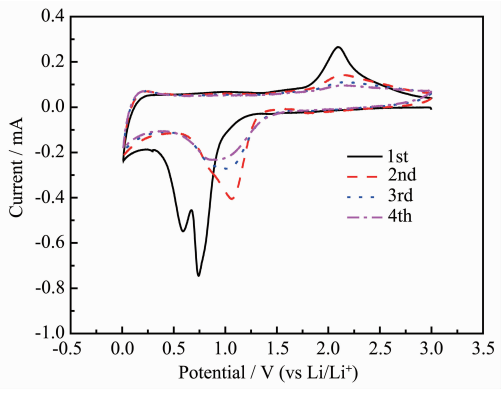

Fig.5　CV curves of Co_3O_4/C electrode using a voltage window of 0.01~3 V at rate of 0.1 mV·s^{-1}

In order to further evaluate the electrochemical performance of the Co_3O_4/C nanocomposite, a constant current discharge/charge reaction was carried out with a constant current density of 200 mA·g^{-1} at a potential range of 0.01 to 3.0 V. Fig.6 showed the charge-discharge curves and compared the cycle performance of Co_3O_4/C with pure Co_3O_4. It can be seen from Fig. 6a that the discharge platform of Co_3O_4/C material appeared at 1.3 and 1.2 V, and the capacity contribution of the 1.2 V platform was large. In addition, the plateau about 2.0 V in charging process could be attributed to the Co_3O_4 reformation, based on the given conversion reaction of $Co_3O_4+8Li^++8e^- \rightleftharpoons 3Co+4Li_2O$[52]. The first discharge and charge specific capacity (1 491.4 and 1 042.4 mAh·g^{1}, respectively) were higher than the theoretical capacity (890 mAh·g^{-1}) due to the initial irreversible lithium consumption and the inevitable formation of the SEI layer. The first cycle coulomb efficiency was only 69.89%. In the second cycle, the discharge and charge specific capacities of the material were 1 106.5 and 1 059.9 mAh·g^{-1}, respectively. Compared with the first cycle, the irreversible capacity loss of the discharge capacity was 384.9 mAh·g^{-1}, and the coulomb efficiency increased to 95.78%. In the next discharge/charge cycles, the curves were almost coincident and the coulomb efficiencies in the 5th, 50th and 100th cycles, were 95.36%, 98.43% and 98.48%, respectively, indicating

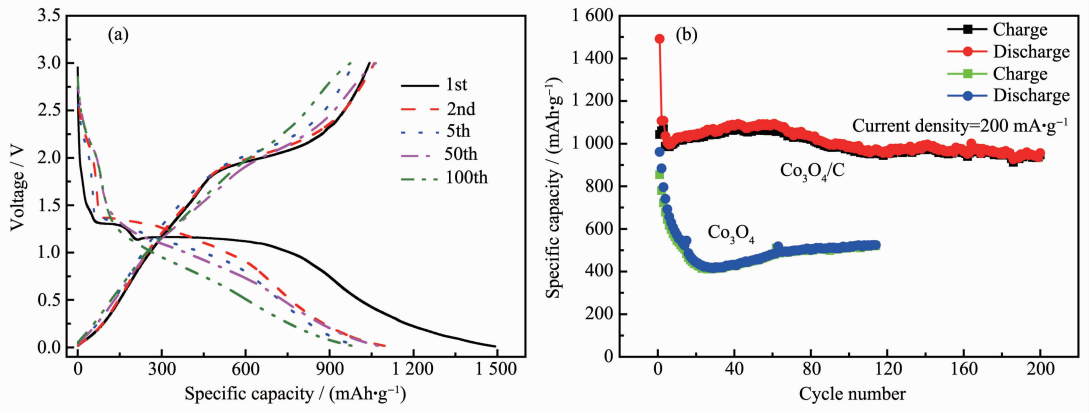

Fig.6　(a) Charge-discharge curves of Co_3O_4/C materials; (b) Cycling performances of Co_3O_4/C composite and pure Co_3O_4 electrode at 200 mA·g^{-1}

that the Co_3O_4/C composites have good reversibility.

The cycle performances of pure Co_3O_4 and Co_3O_4/C composite electrodes at 200 mA·g^{-1} are shown in Fig.6b. The initial specific discharge capacity of the Co_3O_4/C composite electrode was 1 491.4 mAh·g^{-1}, which was still remained at 980 mAh·g^{-1} after 200 cycles. In contrast, despite the higher initial capacity of the Co_3O_4, the subsequent capacity dropped down rapidly to a minimum of 457 mAh·g^{-1} at the 20th cycle. Obviously, under the same experimental conditions, the cycle performance of Co_3O_4/C nanocomposite electrode was significantly better than that of Co_3O_4. This indicated that carbon played a very important role in providing electronic conductive paths and reducing the stress caused by volume changes, ultimately giving the anode a superior performance.

The rate performances of Co_3O_4/C composite and Co_3O_4 are shown in Fig.7. The average discharge capacities of Co_3O_4/C nanocomposite were 1 076.3, 976.2, 872.9, 783.6 and 670.1 mAh·g^{-1} at the current densities of 100, 200, 500, 1 000 and 2 000 mA·g^{-1}, respectively. In addition, when the current density switched back to 100 mA·g^{-1}, the capacity value returned to 1 087 mAh·g^{-1}, showing a good stability. In terms of pure Co_3O_4 electrode, the capacity decayed rapidly as the current density increased. The discharge capacities at 100, 200, 500, 1 000, and 2 000 mA·g^{-1} were 1 057.3, 743.1, 505.8, 355.7 and 243.2 mAh·g^{-1}, respectively. These results demonstrated that the Co_3O_4/C composite not only had better cycle performance, but also had a significantly improved rate performance, which may be due to the important role of carbon played in improving the conductivity and buffering the volume changes during the electrode reaction.

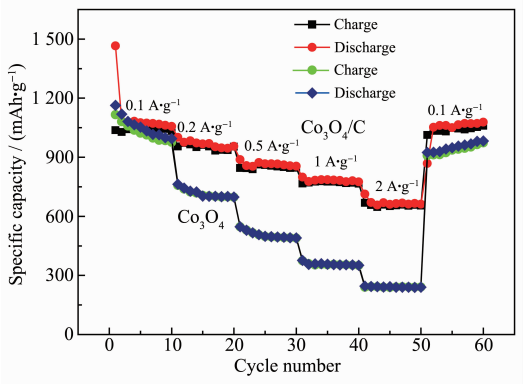

Fig.7 Rate performance of Co_3O_4/C and Co_3O_4 at different current densities

Electrochemical impedance spectroscopy measurements were also conducted for Co_3O_4/C and Co_3O_4 electrodes. The Nyquist plots and corresponding fitting curves based on the inset equivalent circuit were given in Fig.8 and the fitting values were listed in Table S1. In the equivalent circuit, R and R were respectively ohmic resistance (total resistance of the electrolyte, separator and electrical contacts) and charge-transfer resistance[56-57]. CPE was the constant phase angle element, which contained a double layer capacitor, and Z_W represented the Warburg impedance reflecting the solid state diffusion of lithium ion into the bulk of the active materials[56-57]. In general, the smaller the diameter of a semicircle, the lower the charge-transfer resistance of the electrode[57-60]. It could be seen that the semicircular radius of Co_3O_4/C in the high to medium region was significantly smaller than that of pure Co_3O_4, which was in consistent with the fitting result that a smaller R_{ct} values 28.2 Ω for Co_3O_4/C than 46.02 Ω for Co_3O_4, indicating that the charge transfer at the electrode/electrolyte interface was easier, and the reactivity was higher after carbon composting.

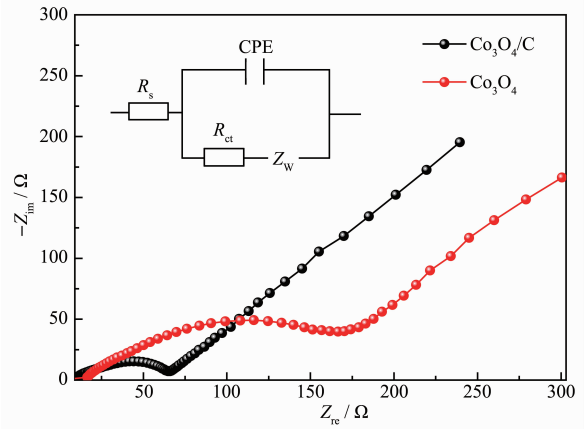

Inset: electrical equivalent circuit

Fig.8 EIS of Co_3O_4/C and Co_3O_4 materials

3 Conclusions

In this study, Co_3O_4/C was fabricated by using $Co_2(NDC)_2(DMF)_2$ as the precursor through a two-step

calcination techniques. It had been found that the Co_3O_4/C composite delivered a high capacity, good cycling stability and rate capability as compared to pure Co_3O_4 counterpart when used as anode for LIBs. In particular, Co_3O_4/C delivered a quite outstanding storage capacity of discharge capacity of 1 000 mAh·g^{-1} after 200 cycles in a current density of 200 mA·g^{-1} and 670 mAh·g^{-1} at a current density of 2 000 mA·g^{-1}. Its good electrochemical performance was attributed to the reasonable choice of organic ligand that provided more carbon in the composite which can efficiently buffer the volume changes of Co_3O_4 during the Li ion insertion/extraction processes and greatly reduce the charge-transfer resistance.

Acknowledgements: This work was supported by the National Natural Science Foundation of China (Grants No. 21103013, 21473014), the Natural Science Foundation of Shanxi Province (Grant No.2016JM5082), Student′s Platform for Innovation and Entrepreneurship Training Program (Grants No. 201810710113, 201910710469).

Supporting information is available at http://www.wjhxxb.cn

References:

[1] Sasaki T, Ukyo Y, Novak P. *Nat. Mater.*, **2013**,**12**:569-575

[2] Ji L, Lin Z, Alcoutlabi M, et al. *Energy Environ. Sci.*, **2011**,**4**:2682-2699

[3] Aricò AS, Bruce P, Scrosati B, et al. *Nat. Mater.*, **2005**,**4**:366-377

[4] Lan D, Chen Y Y, Chen P, et al. *ACS Appl. Mater. Interfaces*, **2014**,**6**:11839-11845

[5] Wei X J, Gou H, Mo Z L, et al. *Ionics*, **2016**,**22**:1197-1207

[6] Simon P, Gogotsi Y, Dunn B. *Science*, **2014**,**343**:1210-1211

[7] Lukatskaya M R, Dunn B, Gogotsi Y. *Nat. Commun.*, **2016**,**7**:12647

[8] Wang G P, Zhang L, Zhang J J. *Chem. Soc. Rev.*, **2012**,**41**:797-828

[9] Mei J, Liao T, Kou L Z, et al. *Adv. Mater.*, **2017**,**29**:1700176

[10]Tummala R, Guduru R K, Mohanty P S. *J. Power Sources*, **2012**,**199**:270-277

[11]Tummala R, Guduru R K, Mohanty P S. *J. Power Sources*, **2012**,**209**:44-51

[12]Marzuki N S, Taib N U, Hassan M F, et al. *Electrochim. Acta*, **2015**,**182**:452-457

[13]Wang Y, Zhang H J, Wei J, et al. *Energy Environ. Sci.*, **2011**,**4**:1845-1854

[14]Shen L S, Wang C X. *Electrochim. Acta*, **2014**,**133**:16-22

[15]Tan Y L, Gao Q M, Yang C X, et al. *Sci. Rep.*, **2015**,**5**:1-11

[16]Reddy M V, Subba Rao G V, Chowdari B V R. *Chem. Rev.*, **2013**,**113**:5364-5457

[17]Lee S H, Sridhar V, Jung J H, et al. *ACS. Nano*, **2013**,**7**:4242-4251

[18]Lin J, Peng Z W, Xiang C S, et al. *ACS. Nano*, **2013**,**7**:6001-6006

[19]Eom J Y, Kwon H S. *ACS Appl. Mater. Interfaces*, **2011**,**3**:1015-1021

[20]Lee H J, Yoo J K, Park J H, et al. *Adv. Energy Mater.*, **2012**,**2**:976-982

[21]Gómez-Cámer J L, Morales J, Sánchez L. *J. Mater. Chem.*, **2011**,**21**:811-818

[22]Wang G R, Wang L, Zhu F L, et al. *Electrochim. Acta*, **2017**,**257**:138-145

[23]Qiu J H, Yu M, Zhang Z H, et al. *J. Alloys Compd.*, **2019**,**775**:366-371

[24]Bala S, Mondal I, Goswami A, et al. *J. Mater. Chem. A*, **2015**,**3**:20288-20296

[25]Tian B B, Ning G H, Gao Q, et al. *ACS Appl. Mater. Interfaces*, **2016**,**8**:31067-31075

[26]Stock N, Biswas S. *Chem. Rev.*, **2012**,**112**:933-969

[27]Tan J C, Civalleri B. *CrystEngComm*, **2015**,**17**:197-198

[28]Zhou H C, Kitagawa S. *Chem. Rev.*, **2014**,**43**:5415-5418

[29]Hu H, Zhang J T, Guan B Y, et al. *Angew. Chem. Int. Ed.*, **2016**,**55**:9514-9518

[30]Jin L N, Zhao X S, Qian X Y, et al. *Mater. Lett.*, **2017**,**199**:176-179

[31]Wang L, Wu J F, Chen Y Q, et al. *Electrochim. Acta*, **2015**,**186**:50-57

[32]Gan Q M, Zhao K M, Liu S Q, et al. *Electrochim. Acta*, **2017**,**250**:292-301

[33]Wang F X, Han Q G, Yi Z, et al. *J. Electroanal. Chem.*, **2017**,**807**:196-202

[34]Li J B, Yan D, Lu T, et al. *Chem. Eng. J.*, **2017**,**325**:14-24

[35]Yang Q, Feng C Q, Liu J W, et al. *Appl. Surf. Sci.*, **2018**,**443**:401-406

[36]Zhuang G L, Gao Y F, Zhou X, et al. *Chem. Eng. J.*, **2017**,**330**:1255-1264

[37]Shao J, Wan Z M, Liu H M, et al. *Mater. Chem.*, **2014**,**2**(31):12194-12200

[38]Zheng S S, Li X R, Yan B Y, et al. *Adv. Energy Mater.*, **2017**,**7**(18):1602733

[39]Qu Q T, Gao T, Zheng H Y, et al. *Carbon*, **2015**,**92**:119-125

[40]Zhu D Q, Zheng F C, Xu S H, et al. *Dalton Trans.*, **2015**,**44**

(38):16946-16952

[41]Han Y, Zhao M L, Dong L, et al. *J. Mater. Chem. A*, **2015**,**3**: 22542-22546

[42]Zhang F, Qi D D, Zhang X G. *Int. J. Electrochem. Sci.*, **2016**,**11**:189-199

[43]Li C, Chen T Q, Xu W J, et al. *J. Mater. Chem. A*, **2015**,**3** (10):5585-5591

[44]Gou L, Ma L, Zhao M J, et al. *J. Mater. Sci.*, **2019**,**54**:1529-1538

[45]Wu Z S, Ren W, Wen L, et al. *ACS Nano.*, **2010**,**4**:3187-3194

[46]Liu J J, Liu H C, Wang F, et al. *RSC Adv.*, **2015**,**5**(110): 90785-90796

[47]Li F, Zhai G H, Ren H J, et al. *Ionics*, **2018**,**24**(1):111-120

[48]Cai T, Huang H, Deng W, et al. *Appl Catal. B*, **2015**,**166**: 393-405

[49]Todorova S, Kolev H, Holgado J P, et al. *Appl Catal. B*, **2010**,**94**:46-54

[50]Dedryvère R, Laruelle S, Grugeon S, et al. *Chem. Mater.*, **2004**,**16**:1056-1061

[51]Biesinger M C, Payne B P, Grosvenor A P, et al. *Appl. Surf. Sci.*, **2011**,**257**:2717-2730

[52]Fang D, Li L C, Xu W L, et al. *J. Mater. Chem. A*, **2013**,**1**: 13203-13208

[53]Zhuang G L, Gao Y F, Zhou X, et al. *Chem. Eng. J.*, **2017**, **330**:1255-1264

[54]Li W Y, Xu L N, Chen J. *Adv. Funct. Mater.*, **2005**,**15**:851-857

[55]Zhao Y, Huang Y, Wang Q F, et al. *Electron. Mater. Lett.*, **2013**,**9**:683-686

[56]Yang S Z, Cui G L, Pang S P, et al. *ChemSusChem*, **2010**,**3**: 236-239

[57]Zhu G, Jiao B J, Li J T. *Mater. Res. Innovations*, **2014**,**18** (7):528-534

[58]Slepski P, Darowicki K, Janicka E, et al. *J. Solid State Electrochem.*, **2012**,**16**:3539-3549

[59]Park S J, Kim Y J, Lee H. *J. Power Sources*, **2011**,**196**:5133-5137

[60]Yang Q, Feng C Q, Liu J W, et al. *Appl. Surf. Sci.*, **2018**,**443**: 401-406